

**RESEARCH ARTICLE**

# Nonlinear dynamic modeling and model predictive control of thrombin generation to treat trauma-induced coagulopathy

Damon E. Ghetmiri<sup>1</sup> | Amor A. Menezes<sup>\*1,2,3</sup>

<sup>1</sup>Department of Mechanical and Aerospace Engineering, University of Florida, Florida, United States of America

<sup>2</sup>J. Crayton Pruitt Family Department of Biomedical Engineering, University of Florida, Florida, United States of America

<sup>3</sup>Department of Agricultural and Biological Engineering, University of Florida, Florida, United States of America

**Correspondence**

\*Corresponding author: Amor Menezes.  
Email: amormenezes@ufl.edu

**Present Address**

Department of Mechanical and Aerospace Engineering, University of Florida, 527 Gale Lerner Drive, Gainesville, FL 32611-6250, USA

**Summary**

This article is motivated by the pressing need to robustly automate clinical interventions for trauma-induced coagulopathy (TIC). TIC occurs after severe trauma and shock, and has poor outcomes and about 30% mortality. Although modulating the blood proteins that drive TIC can improve patient outcomes, no practical control-oriented methodology exists to accurately capture biochemical process dynamics and satisfactorily regulate clotting. Hence, we propose a nonlinear dynamic coagulation model that distills the complex biochemical reactions of clotting and also simultaneously generalizes an existing linear phenomenological model. Using our new nonlinear model, we demonstrate the feasibility of model predictive control (MPC) to automate clinical treatments, first in a single-input case that is similar to current open-loop clinical practice, and second in a multi-input case that administers three blood proteins as system inputs to attain satisfactory TIC treatment. The output in both cases is the key clotting protein thrombin. To test robustness, we confirm that both single-input and multi-input MPC are suitable for TIC treatment in the presence of an experimentally-observed nonlinearity, an unknown state-dependent power law input delay. Thus, this article provides a strong foundation to transition current open-loop clinical approaches to closed-loop process control.

**KEYWORDS:**

nonlinear systems, model predictive control, systems biology, control applications, trauma coagulopathy

## 1 | INTRODUCTION

Precision medicine<sup>1</sup> to resuscitate trauma patients<sup>2</sup> is desirable because trauma remains the leading cause of death between the ages of 1–44 in the U.S.<sup>3</sup>, with per capita numbers on the rise<sup>4</sup>. Trauma patients who survive suffer huge morbidity and permanent disabilities<sup>5</sup>. Trauma-induced coagulopathy (TIC)<sup>6</sup> is a condition that results when shock accompanies severe trauma. This condition is biologically characterized by a disruption to the balance between clot formation and fibrinolysis (clot degradation)<sup>7</sup>, and is clinically characterized by uncontrolled bleeding that leads to either death or clotting complications in those who survive<sup>8,9,10</sup>. An example of precision medicine for trauma patients is the tailoring of transfusions to deliver beneficial coagulation factor (blood protein) concentrates<sup>8,7</sup>. This approach is unlike current resuscitation strategies that rapidly administer uncharacterized blood products to control hemorrhage<sup>11</sup>. Tailored approaches offer a way to reduce a still-high massive transfusion mortality rate of about 30%<sup>12</sup>, a rate that has not decreased despite recent modifications to non-personalized resuscitation protocols<sup>13</sup>.

The coagulation cascade<sup>14</sup> is a network of complex biochemical reactions of coagulation factors that interact to form a clot to stop hemorrhage. This network is triggered by tissue factor (TF) after injury, which leads to the production of a key clotting protein

called thrombin, factor IIa. (As is convention, we use a lower-case ‘a’ after a coagulation factor’s Roman numeral designation to denote its active form.) Thrombin is the end product of the coagulation cascade, and functions as both a procoagulant and an anticoagulant<sup>15</sup>. Coagulation factors in the coagulation cascade regulate the concentration of thrombin that is output by the system<sup>14</sup>. Thus, administering coagulation factor concentrates as either individual therapeutics or in cocktail combinations has benefit, for instance, in hematologic diseases such as hemophilia<sup>16,17</sup>. Indeed, targeted coagulation factor therapy can have better outcomes compared to administering uncharacterized blood products<sup>18,19,20</sup>. Examples of targeting include using factor VII<sup>21</sup> and factor IX<sup>22</sup> to correct coagulopathic hemorrhage, and factor X as an anticoagulant to prevent and treat thromboembolic events<sup>23</sup>.

We have shown that coagulation factor concentrations equilibrate in the first 24 hours of a trauma patient recovery trajectory, toward values that are considered to be normal<sup>24</sup>. We have also shown that each coagulation factor concentration has a unique effect on clotting system dynamics<sup>24</sup>. Moreover, it is relatively quick, approximately five minutes, to simultaneously measure multiple coagulation factor concentrations in a blood sample using existing devices. Therefore, trauma patients may benefit from a treatment approach that administers multiple coagulation factor concentrations to regulate recovery. To accomplish this goal treatment, we can harness dynamical system models that mediate between coagulation kinetics and physiological trauma measures. In the few studies that mathematically generate the concentration time-history of thrombin from measured coagulation factor concentrations, either the models are linear with states that are not experimentally measurable<sup>25</sup>, or their computational loads are high<sup>26</sup>, which precludes model use in urgent care settings. Since we have previously shown that coagulation factor concentration modulation approaches have merit<sup>24</sup>, and that it is possible to compensate for unique coagulation nonlinearities when tracking a desired reference concentration of thrombin<sup>27</sup>, what remains is the development of a viable process control strategy that harnesses an accurate nonlinear model of experimentally-measurable states. This will enable future experimental validation. Developing such a practical, mechanistic coagulation model along with a closed-loop protein-delivery control strategy, as in this work, will help transition current open-loop clinical interventions to personalized, automated, and robust treatment.

The process control strategy that we implement here is model predictive control (MPC)<sup>28</sup>, a well-established, pervasive regulation method that solves an optimization problem online to determine, at a sample time, the best control actions for a finite horizon. A canonical biomedical engineering example of MPC use is to regulate insulin delivery to diabetic patients<sup>29,30</sup>. MPC is widespread and popular because it can handle constraints well and also accommodate nonlinearities<sup>31</sup>. Both features are important for the application in this article because: (1) the coagulation cascade is an example of a positive dynamical system, with states that are confined to the positive orthant of  $\mathbb{R}^n$ , which is denoted in this article by  $\mathbb{R}^+$ ; and (2) the coagulation process is subject to characteristic nonlinearities that must be compensated for, including an unknown state-dependent power law input delay and input saturation<sup>27</sup>. When coupled with MPC’s potential to adapt to uncertainty<sup>32</sup>, such as that arising from patient variability, the technique represents a promising process control approach for TIC treatment. Moreover, MPC use can be extended to coagulopathy disorders beyond TIC, for example, hemophilia, factor V Leiden, von Willebrand disease, and coagulation factor deficiencies.

This article proposes a nonlinear dynamic coagulation model and demonstrates the feasibility of personalizing TIC treatment via MPC. Our intellectual contributions include:

1. A novel nonlinear coagulation model that accurately captures coagulation cascade process dynamics. This model is superior to the sole existing control-oriented phenomenological linear coagulation model in the literature, since each state in our new dynamical system is an individual coagulation factor instead of a protein complex that is not experimentally measurable and that hence cannot be sensed in a closed-loop TIC treatment scheme. That is, our new nonlinear model improves system observability and controllability.
2. An *in silico* feasibility demonstration of MPC for TIC treatment. Here, MPC is used in a single-input single-output (SISO) scheme to regulate thrombin generation in a manner that automates current clinical practice, and is also used in a multi-input single-output (MISO) scheme that leverages the structure of our nonlinear model to manipulate different coagulation proteins simultaneously.
3. A confirmation of controller robustness in both SISO and MISO schemes, to compensate for unmodeled nonlinearities such as the aforementioned unknown state-dependent power law input delay.

The remainder of this article is as follows. Section 2 develops the nonlinear coagulation model and articulates its stoichiometric intuition. Section 3 shows the feasibility of regulating thrombin generation with MPC akin to how clinicians currently intervene in trauma patients to accomplish thrombin control. Section 4 extends our MPC controller by leveraging the unique structure of our nonlinear coagulation model. Section 5 evaluates controller performance in the presence of an input nonlinearity, an unknown state-dependent power law time delay, against a state-of-the-art controller that we previously designed using a Lyapunov analysis. Section 6 presents conclusions and future work.

## 2 | A NONLINEAR THROMBIN DYNAMICS MODEL

### 2.1 | Modeling Background

The only control-oriented coagulation model in the literature is a simple linear one that captures thrombin generation effectively<sup>25</sup>. We recently improved this model by incorporating changes to its structure and refining parameters with additional measurement data<sup>24</sup>. The state space representation of this model is:

$$\begin{aligned}\dot{x}_1(t) &= x_2(t) - a_2 x_1(t), \\ \dot{x}_2(t) &= x_3(t) - a_1 x_1(t), \\ \dot{x}_3(t) &= -a_0 x_1(t) + bv(t - \tau),\end{aligned}\tag{1}$$

where  $v(t)$  is a time-delayed input concentration of tissue factor (TF),  $\tau \in \mathbb{R}^+$  is the time delay, and  $b, a_0, a_1,$  and  $a_2 \in \mathbb{R}^+$  are positive model constants. In this canonical completely observable realization, state  $x_1(t)$  is the observed output, i.e., the time-history of thrombin concentration. States  $x_2(t)$  and  $x_3(t)$  are inferred<sup>25</sup> as the concentration time-history of the protein complex Xa-Va (factor Xa bound to factor Va), and the concentration time-history of the protein complex TF-VIIa (TF bound to factor VIIa), respectively. A transfer function representation of (1) from input TF concentration to output thrombin concentration is:

$$\frac{Y(s)}{U(s)} = \left( \frac{K_p}{s + p} \right) \left( \frac{\omega_n^2}{s^2 + 2\zeta\omega_n + \omega_n^2} \right) e^{-\tau s},\tag{2}$$

where  $K_p, p, \zeta, \omega_n,$  and  $\tau$  are patient-specific constants,  $Y(s)$  is the output thrombin concentration time-history in the frequency ( $s$ ) domain, and  $U(s)$  is the input TF concentration time-history in the frequency domain.

Despite the efficacy of model (1) in predicting thrombin generation, it has the following deficiencies.

1. The model consists of terms that have little biochemical kinetic meaning, since it is phenomenological.
2. The model is limited by the fact that its inferred system states are protein complexes (Xa-Va and TF-VIIa), for which no experimental measurement technique exists.
3. The model precludes a practical multi-input controller, since protein complexes are not available for administration.
4. The model states can take on negative values since there are no explicit state constraints; however, negative values contradict the physical meaning of the system, because protein concentrations cannot be negative.

Thus, this model is not suitable for applications beyond single-input TF-based control.

### 2.2 | Nonlinear Model Development

To address the limitations of model (1) and to better capture coagulation nonlinearities, we develop a nonlinear model below that has states of individual coagulation factor concentrations. Such a model permits the use of intermediate coagulation factor concentrations as system inputs, and bypasses the measurement inadequacies of protein complexes. Moreover, we have previously shown that individual coagulation factors uniquely affect coagulation dynamics<sup>24</sup>. Therefore, leveraging these effects will improve system performance. Hence, our nonlinear model will be more observable and controllable than (1), and thus more practical.

We consider the primary coagulation factors that drive the extrinsic and common pathways of the coagulation cascade, namely, TF and factors II, VII, and X. The fundamental biochemical reactions that drive thrombin generation comprise the release of TF upon injury, the resultant activation of existing factor VII in the body by the complex TF-VIIa, and the subsequent activation of factor X that then drives the activation of factor II and generates thrombin. For a single-input case with TF as the only system input, these mechanisms can be represented in the following state-space form:

$$\dot{x}_1(t) = -K_{d_1} x_1(t) - \beta x_1(t)x_2(t) + u(t - \tau),\tag{3a}$$

$$\dot{x}_2(t) = K_{p_2} - K_{d_2} x_2(t) - \beta x_1(t)x_2(t),\tag{3b}$$

$$\dot{x}_3(t) = \gamma x_1(t)x_2(t) - K_{d_3} x_3(t),\tag{3c}$$

$$\dot{x}_4(t) = K_{n_4} x_3(t) - K_{d_4} x_4(t),\tag{3d}$$

where  $\mathbf{x}(t) \in \mathbb{R}^4$  is a vector of system states, for which the concentrations of TF, factor VII, factor Xa, and factor IIa (thrombin) are the corresponding states, respectively;  $K_{d_i} \in \mathbb{R}^+, i = 1, 2, 3, 4,$  are the degradation rates of the respective coagulation factors;

$K_{p_2} \in \mathbb{R}^+$  is the production rate of factor VII in the body;  $\beta \in \mathbb{R}^+$  is the sequestration rate of TF and of factor VII because of the formation of the TF-VII complex;  $\gamma \in \mathbb{R}^+$  is the activation of factor X induced by TF-VIIa, assumed proportional to TF-VII; and  $\tau \in \mathbb{R}^+$  is an input delay.

We explicitly convert the state space representation of the coagulation model (3) to a biochemical kinetics representation through the reaction equations in Table 1, with further explanation in Table 2. Table 1 also compares our model to the ‘‘gold standard’’ Hockin-Mann stoichiometric model of blood coagulation<sup>33</sup>, and confirms phenomenological equivalence.

**TABLE 1** Biochemical Kinetics of Our Coagulation Model (3)

Eq.	State	Differential Equation	Simplified Kinetics	Relevant Hockin-Mann Model Kinetics <sup>33</sup>
(3a)	TF	$\dot{x}_1 = -K_{d_1}x_1 - \beta x_1x_2$	$\text{TF} \xrightarrow{K_{d_1}} \emptyset$ $\text{TF} + \text{VII} \xrightarrow{\beta} \text{TF-VII}$	$\text{TF} + \text{VII} \rightleftharpoons \text{TF-VII}$ $\text{TF} + \text{VIIa} \rightleftharpoons \text{TF-VIIa}$ $\text{TF-VIIa} + \text{VII} \rightarrow \text{TF-VIIa} + \text{VIIa}$
(3b)	VII	$\dot{x}_2 = K_{p_2} - K_{d_2}x_2 - \beta x_1x_2$	$\emptyset \xrightarrow{K_{p_2}} \text{VII}$ $\text{VII} \xrightarrow{K_{d_2}} \emptyset$ $\text{TF} + \text{VII} \xrightarrow{\beta} \text{TF-VII}$	
(3c)	Xa	$\dot{x}_3 = \gamma x_1x_2 - K_{d_3}x_3$	$\text{Xa} \xrightarrow{K_{d_3}} \emptyset$ $\text{TF} + \text{VII} \xrightarrow{\gamma} \text{Xa}$	$\text{TF-VIIa} + \text{X} \rightleftharpoons \text{TF-VIIa-X} \rightarrow \text{TF-VIIa-Xa}$ $\text{TF-VIIa} + \text{Xa} \rightleftharpoons \text{TF-VIIa-Xa}$
(3d)	IIa	$\dot{x}_4 = K_{n_4}x_3 - K_{d_4}x_4$	$\text{IIa} \xrightarrow{K_{d_4}} \emptyset$ $\text{Xa} \xrightarrow{K_{n_4}} \text{IIa}$	$\text{Xa} + \text{II} \rightarrow \text{Xa} + \text{IIa}$ $\text{Xa} + \text{Va} \rightleftharpoons \text{Xa-Va}$ $\text{Xa-Va} + \text{II} \rightleftharpoons \text{Xa-Va-II} \rightarrow \text{Xa-Va} + \text{mIIa}$ $\text{mIIa} + \text{Xa-Va} \rightarrow \text{IIa} + \text{Xa-Va}$

**TABLE 2** Phenomenological Explanation of Key Terms in Model (3)

Term	Explanation
$-\beta x_1x_2$	Formation of complex TF-VII.
$\gamma x_1x_2$	Formation of complex TF-VIIa proportional to TF-VII. The TF-VIIa complex activates factor X.
$K_{n_4}x_3$	Direct activation of factor II by factor Xa, and indirect activation of factor II by forming the complex Xa-Va and another intermediate, mIIa.

A typical equilibrium in healthy individuals is  $x_1 = 0$ ;  $x_2 = x_{2_0}$ ;  $x_3 = 0$ ; and  $x_4 = 0$ , where  $x_{2_0}$  is the initial concentration of factor VII. That is, the concentration of factor VII at equilibrium is its initial constant positive value, with all other equilibrium coagulation factor concentrations being zero<sup>33</sup>. It follows that the model (3) parameters must satisfy  $K_{p_2} = x_{2_0}K_{d_2}$ .

Linearizing around this typical equilibrium and applying the Laplace transform, we obtain a transfer function for model (3) as:

$$\frac{Y(s)}{U(s)} = \frac{\gamma K_{p_2} K_{n_4}}{(s + K_{d_3})(s + K_{d_4})(K_{d_2}s + K_{d_1}K_{d_2} + \beta K_{p_2})} e^{-\tau s}, \quad (4)$$

where  $Y(s)$  is the output thrombin concentration time-history in the frequency domain, and  $U(s)$  is the input TF concentration time-history in the frequency domain. Define:

- $K_0 = K_{d_1}K_{d_3}K_{d_4} + \beta K_{d_3}K_{d_4}x_{2_0}$ ;
- $K_1 = K_{d_1}K_{d_3} + K_{d_1}K_{d_4} + K_{d_3}K_{d_4} + \beta K_{d_3}x_{2_0} + \beta K_{d_4}x_{2_0}$ ;
- $K_2 = K_{d_1} + K_{d_3} + K_{d_4} + \beta x_{2_0}$ ;

- $K_n = \gamma K_{n_4} x_{2_0}$ .

Then the transfer function (4) simplifies to

$$\frac{Y(s)}{U(s)} = \frac{K_n}{s^3 + K_2 s^2 + K_1 s + K_0} e^{-\tau s}. \quad (5)$$

This transfer function (5) of our linearized nonlinear model is a third order transfer function that recovers (2) exactly, the transfer function of the linear model presented in the literature<sup>25,24</sup>. This recovery supports the Akaike Information Criterion result in the literature<sup>25,24</sup> that (2) is the simplest informative model for thrombin generation.

To confirm that our nonlinear model captures the mechanistic essence of coagulation, we contrasted its fit of experimental thrombin data to the linear model in the literature<sup>25,24</sup>. We used the MATLAB Simulink Design Optimization toolbox to fit our model to experimental thrombin data generated by Calibrated Automated Thrombogram (CAT)<sup>34</sup> tests on samples of the plasma of 20 normal individuals<sup>25</sup> for 5 pM of TF impulse input, Dataset 1. The mean fit  $R^2$  value improved from 0.9917 in the linear case to 0.9982 in the nonlinear case.

There is little visual difference in the output of the two models. Consider the simulated thrombin response for an impulse input of TF at the 1 pM, 3 pM, and 5 pM concentration levels for one of these samples. Figure 1 shows the closely comparable results between the nonlinear model (3) and the linear model (1). Thus, the nonlinear model also effectively captures coagulation dynamics, but simultaneously facilitates multi-input coagulation factor control via additional inputs of factors VII and Xa.

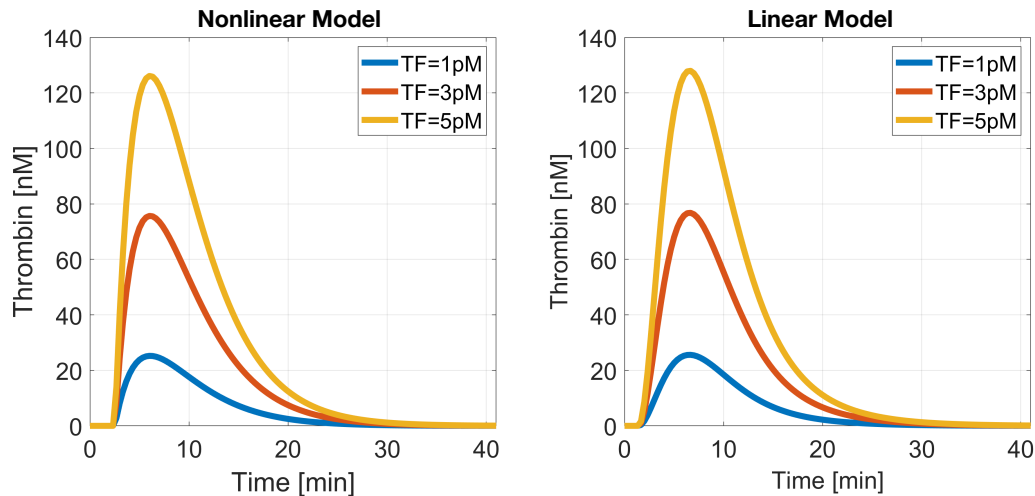


**FIGURE 1** The output of our proposed nonlinear model matches that of the existing linear coagulation model<sup>24</sup>. (A) Thrombin generation as the output of the nonlinear model (3) for different TF impulse inputs. These are comparable to panel (B), the output from the linear model (1). This performance shows that the nonlinear model developed here is able to effectively capture coagulation system dynamics.

To further justify our use of the nonlinear model (3), we show that it captures important problem phenomena under circumstances where the linear model (1) breaks down, specifically, when the linear model inaccurately represents intermediate system states. We use a dataset of measurements that were conducted on samples of plasma from 40 trauma patients<sup>25</sup>, Dataset 2. For illustration, we pick an exemplar trauma patient sample and fit the parameters of the linear (1) and the nonlinear (3) models to the sample's CAT experiment data. Next, because coagulation factors will be physically administered to a patient as a sequence of impulses during treatment, we illustrate each system's response to a pulsed input signal. The response of the fitted linear model is in Figure 2A–D, and the response of the fitted nonlinear model is in Figure 2E–I. The pulse input to both models is identical, Figure 2A and E. Unsurprisingly given Figure 1, the thrombin output from both models is similar, Figure 2B and F. However, the states  $x_1$  and  $x_2$  in the linear model take on negative values, Figure 2C and D, respectively. This response is incorrect because protein complex concentrations cannot physically be negative. In contrast, the concentration states of the nonlinear model stay positive and physically realistic, Figure 2G–I.

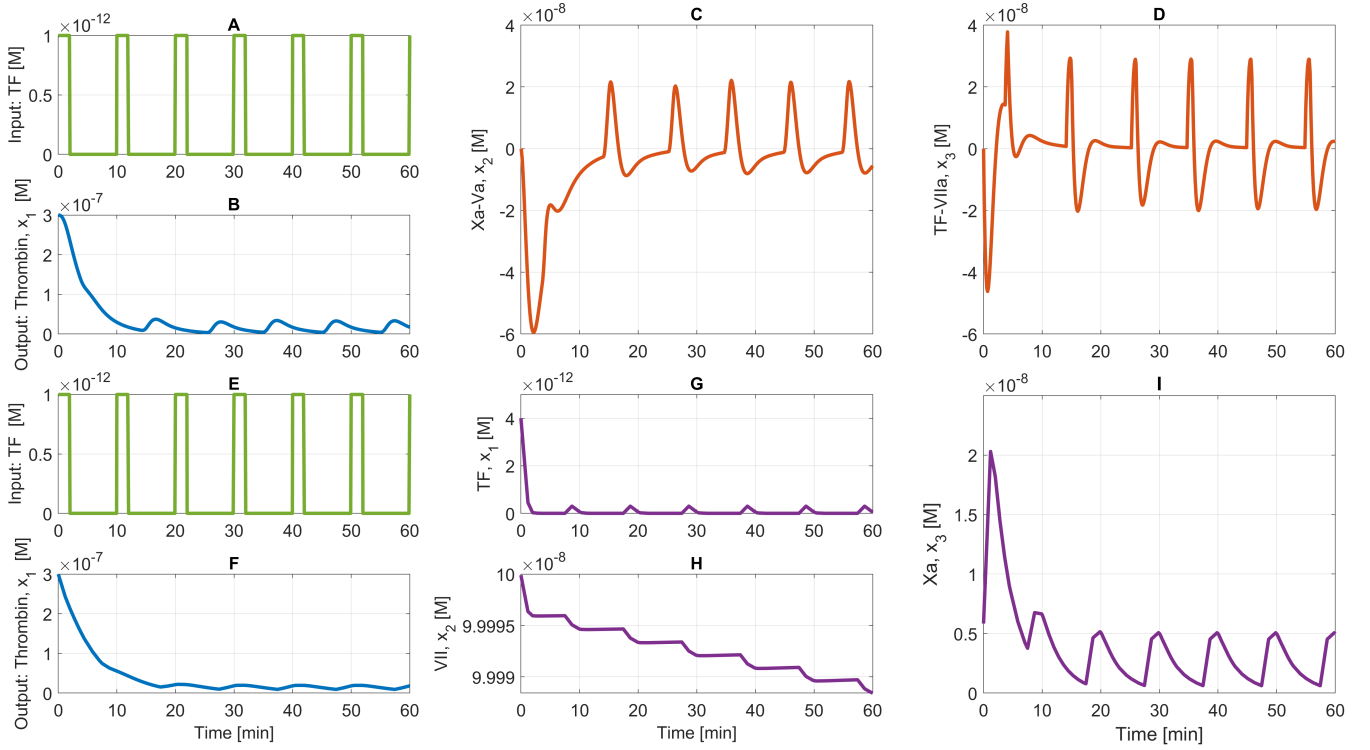


**FIGURE 2** Our proposed nonlinear coagulation model captures important problem phenomena that the existing linear model<sup>24</sup> does not. (A), (E) An identical pulsed TF concentration is input to the linear and nonlinear model, respectively. Each model has parameters that result from a fit to the CAT data that was measured from a trauma patient’s plasma sample. (B), (F) A similar thrombin concentration is output by the linear model (state  $x_1$  of (1)), and the nonlinear model (state  $x_4$  of (3)), respectively. (C) State  $x_2$  and (D) state  $x_3$  of the linear model take on negative values. This violates system practicality, because negative protein complex concentrations are not physically realistic. (G) State  $x_1$ , (H) state  $x_2$ , and (I) state  $x_3$  of the nonlinear model stay positive and physically realistic.

### 3 | SINGLE-INPUT SINGLE-OUTPUT MODEL PREDICTIVE CONTROL

We investigate the feasibility of MPC to treat TIC such that output thrombin levels are regulated by input TF. This SISO scheme will automate current open-loop clinical treatment practice, where coagulation measurements like the CAT, which is generated by a TF input, are obtained from a patient plasma sample and fed to the patient’s operating room, whereupon clinician gestalt and rules-of-thumb are used to administer large volumes of uncharacterized, non-tailored blood products to remedy the observed CAT.

#### 3.1 | ARX Process Model Development

Section 2 contains a nonlinear “truth” model for thrombin generation in trauma patients, because it gives identical results to a linear model that has been validated for trauma. We do not consider the gold standard Hockin-Mann model<sup>33</sup> as a truth model because it has not been validated for trauma. Since model (3) serves as our system plant, and we assume that accurate knowledge of an individual’s coagulation is not known *a priori*, we must perform identification of a typical (healthy normal) coagulation system to obtain a process model for control design. We choose to identify a linear autoregressive with exogenous terms (ARX) model that approximates the relationship between TF and thrombin levels. This ARX model will be the internal model in our MPC scheme to predict coagulation output. For this study, we denote the input TF as  $u(t)$  and the output thrombin as  $y(t)$ , where  $t$  is now the time step index. Figure 3 shows the structure of our MPC setup.

An ARX model that facilitates this relationship approximation between input and output is

$$y(t) + a_1y(t-1) + a_2y(t-2) + \dots + a_{n_a}y(t-n_a) = b_1u(t) + b_2u(t-1) + \dots + b_{n_b}u(t-n_b+1) + w(t), \quad (6)$$

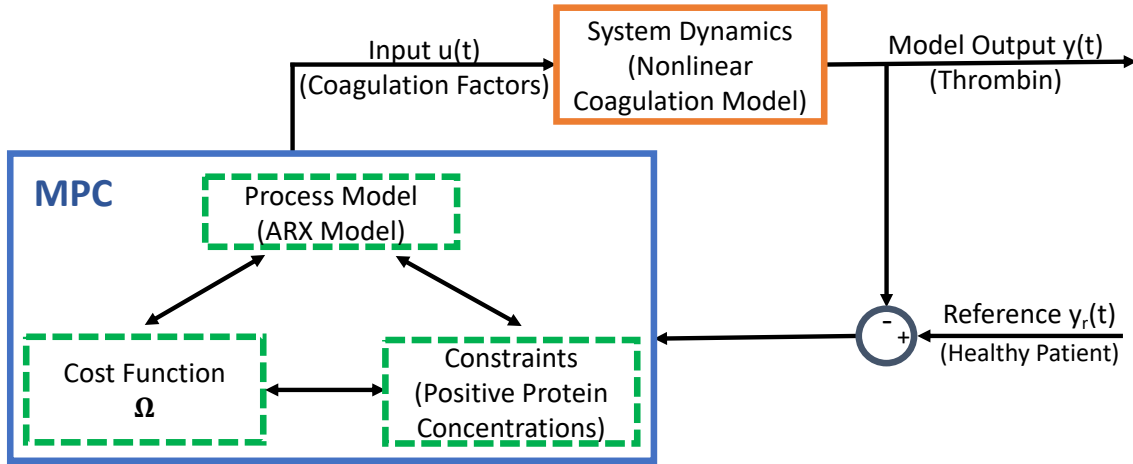


**FIGURE 3** MPC in a closed-loop architecture to treat TIC. The system dynamics (plant) is the nonlinear model (3) that was established in Section 2. Our MPC structure aims to track a reference signal closely, and has three components: a simplified process model to estimate the plant output, problem constraints, and a cost function to optimally solve the control problem. The solution to this problem is a control sequence of coagulation factor concentrations, e.g., TF concentration, that is sent to the system.

where  $n_a$  is the number of past output terms;  $n_b$  is the number of past input terms;  $y(t-i) \forall i \in \{0, 1, \dots, n_a\}$  and  $u(t-i) \forall i \in \{0, 1, \dots, n_b-1\}$  are delayed output and input variables, respectively; and  $w(t)$  denotes uncertainties and disturbances. The  $n_a$  and  $n_b$  values are unrelated to the order of the physical system that model (6) represents. Equation (6) implies that the current output  $y(t)$  is predicted as a weighted sum of past output values and current and past input values, which can be simplified to

$$A(z^{-1})y(t) = B(z^{-1})u(t - n_k) + w(t), \quad (7)$$

where  $z^{-1}$  is a time shift operator, i.e.,  $z^{-1}u(t) = u(t-1)$ , and  $n_k$  denotes the input delay.  $A$  and  $B$  are mapping functions such that  $A(z^{-1}) = \sum_{i=0}^{n_a} a_i(z^{-1})^i$ , where  $a_i \in \mathbb{R}$  are constants and  $a_0 = 1$ , and  $B(z^{-1}) = \sum_{i=1}^{n_b} b_i(z^{-1})^{i-1}$ , where  $b_i \in \mathbb{R}$  are constants.

On the aforementioned experimental dataset of CATs of 20 normal plasma samples, Dataset 1, we calculated the maximum, minimum, and mean of experimental data values at each time point for all normal plasma samples, and fit model (3) to this data. Consequently, we determined a target CAT profile and an associated region inside which any CAT trajectories are normal, Figure 4. Next, we identified an ARX model by performing black-box system identification on the input-output data of the target CAT using the MATLAB System Identification Toolbox with a sampling time of 20 seconds, which is the sampling time of the CAT measurement device. The underlying coagulation dynamics in these experiments includes nonlinearities and noise, which are not fully captured by our simplified models (3) and (5). Hence, despite having *a priori* knowledge of linearized system dynamics, the ARX model order may not correspond to the number of poles of this system due to the unmodeled nonlinearities and noise<sup>35,36</sup>.

To obtain an accurate model without overparameterizing, we selected the simplest model with  $R^2 > 0.9$ :

$$A(z) = 1 - 3.384z^{-1} + 4.607z^{-2} - 3.269z^{-3} + 1.282z^{-4} - 0.2344z^{-5}. \quad (8)$$

$$B(z) = 0.2237z^{-6}. \quad (9)$$

In this model,  $n_a = 5$ ,  $n_b = 1$ , and  $n_k = 6$ . We obtained  $n_a = 5$  and  $n_b = 1$  as an accurate model without overparameterization because  $R^2 = 0.7318$  when  $n_a = 4$  and  $n_b = 1$ , and  $R^2 = 0.9107$  when  $n_a = 5$  and  $n_b = 1$ .

Figure 4A shows that the above identified ARX model produces a CAT that represents normal coagulation because its output remains inside our stipulated normal region. We also performed five-fold cross-validation<sup>37</sup> on ARX model learning, a process that bootstraps available data by subdividing it so that 80% is used for training and the remaining 20% is used for validation. This process is iterated five times for five unique divisions (folds) of the original dataset. We calculated the mean percent error of three CAT parameters (peak, peak-time, and area under the curve) for each fold by comparing each validation CAT parameter (from experiments) to the CAT parameters produced by the learned ARX model of that fold. The mean model output properties of these five iterations on our dataset of 20 normal samples are in Figure 4B. This figure confirms good prediction capability. Obtaining errors of 20% or less is a rule-of-thumb for mechanical systems, with less than 10% the ultimate goal through model refinement<sup>38</sup>; given significant inherent biological variability compared to mechanical systems and possible as-yet-undiscovered

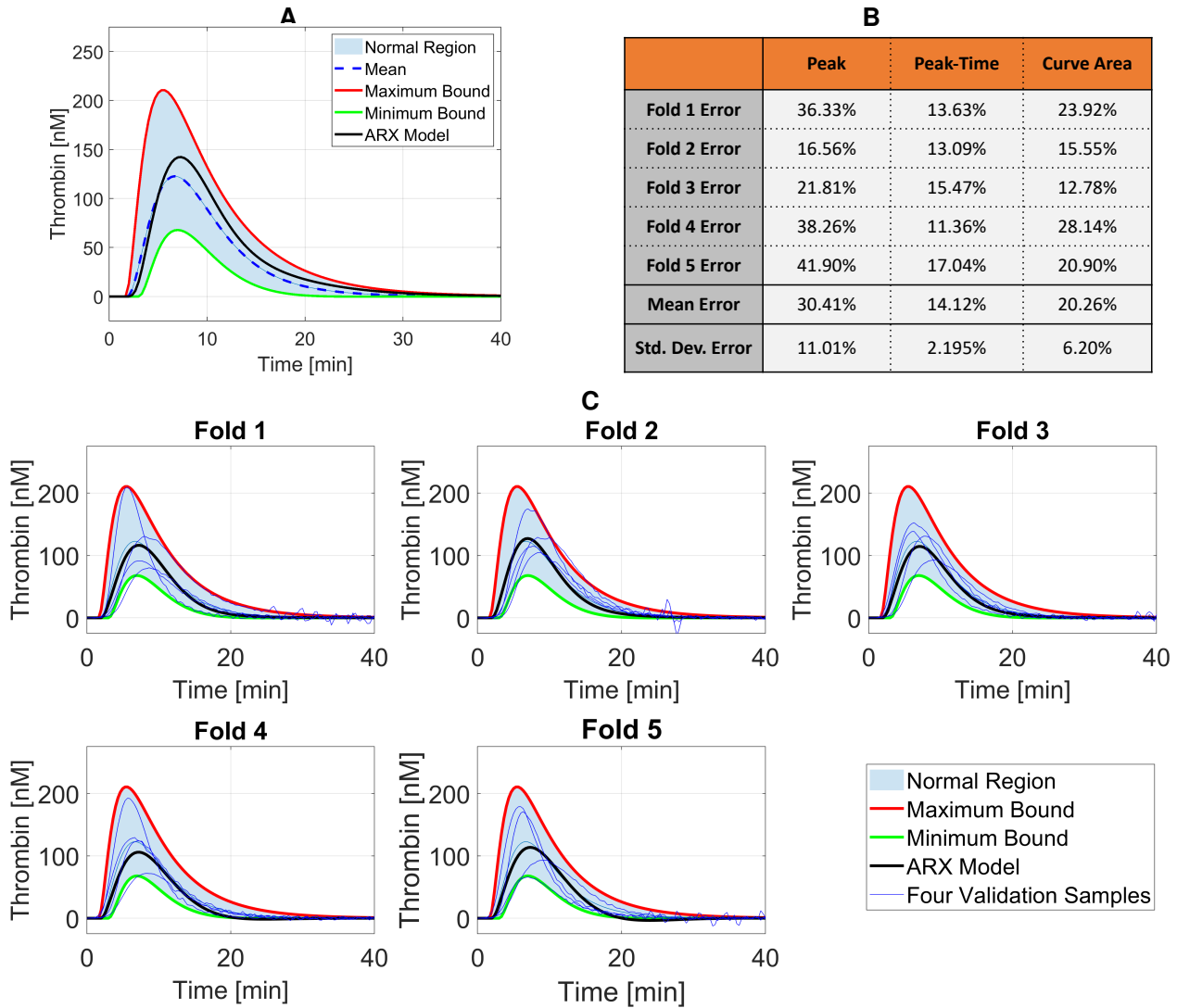


**FIGURE 4** Normal thrombin generation, an ARX model of this normal, and five-fold cross-validation of this ARX model. (A) We identified a normal CAT region using experimental CAT measurements on plasma samples from 20 normal donors. The region's mean and bounds were determined by fitting model (3) to the mean, minimum, and maximum of all experimental data at each time point. This region is chosen between candidate options<sup>24</sup> because it offers the best representation of the data, and is the most restrictive. The black line indicates the output of the ARX model (8) learned on the mean normal CAT. (B) Five-fold cross-validation bootstraps the data from the 20 normal plasma samples. We report the mean percent error of three CAT parameters for each fold, and the mean and standard deviation of all sample relative errors. For example, CAT Peak percent error =  $\left| \frac{\text{Peak}_{\text{model}} - \text{Peak}_{\text{experiment}}}{\text{Peak}_{\text{experiment}}} \right| \times 100$ . (C) The validation CAT samples and the trained ARX model of each fold. This panel confirms that the ARX model structure is valid for use as an MPC process model.

interactions, a target of 30% or less error is not unreasonable. Figure 4C depicts the validation CAT data and the learned ARX model of each fold. This learned ARX model is always within the stipulated normal region.

### 3.2 | Model Predictive Control Design and Performance

Defining  $y_r(t)$  to be a desired normal thrombin profile that a trauma patient should recover to, our control objective is for output  $y(t)$  to track reference  $y_r(t)$  as closely as possible, i.e., we want tracking error  $e(t) = y_r(t) - y(t)$  to go to zero as  $t \rightarrow \infty$ . Our

MPC scheme has the conventional three key components: a prediction model, a cost function, and receding horizon optimization. We use the ARX model (7) for our prediction model.

We choose the cost function

$$\Omega \triangleq \sum_{k=1}^N \alpha_1 (y_r(t+k) - \hat{y}(t+k|t))^2 + \sum_{i=0}^M \left[ \alpha_2 (u(t+i|t))^2 + \alpha_3 (\Delta u(t+i|t))^2 \right], \quad (10)$$

where the integers  $N$  and  $M$  ( $N > M$ ) are referred to as the prediction horizon and control horizon, respectively. In (10),  $\hat{y}(t+k|t)$  denotes the estimate value of  $y(t+k)$  based on knowledge at time  $t$ ,  $u(t+i|t) \forall i = 0, 1, \dots, M$  are possible control sequences over the control horizon, and  $\Delta u$  denotes the change in the control signal over time. Hence, the controller update law is

$$\Delta u(t+i|t) = u(t+i) - u(t).$$

Also in (10),  $\alpha_1$ ,  $\alpha_2$ , and  $\alpha_3$  are weights of the cost function that adjust the relative importance of the penalty from the components' tracking error, input, and input variation, respectively. Weight  $\alpha_1$  ensures that the thrombin output closely tracks the desired reference. Weight  $\alpha_2$ , the input penalty weight, ensures that the control sequence does not deviate excessively from the nominal input value. For instance, in a healthy uninjured individual, the TF concentration in blood is zero<sup>33</sup>. Therefore, to move a trauma patient toward normal, we set the nominal value of the input to zero. Because of our  $\alpha_2$  weight, the optimization solver will attempt to find a minimum TF concentration. Weight  $\alpha_3$  ensures that there is no drastic change from one control sequence to another, to prevent shocks in the coagulation system response. We select the weights of the objective cost function in (10) as

$$\alpha_1 = 1, \alpha_2 = 0.5, \text{ and } \alpha_3 = 0.3.$$

Because the coagulation system is a biochemical instance of a positive system, the system states are confined to the positive orthant. Thus, a negative input or output is meaningless in coagulopathy treatment, i.e., proteins cannot be removed from the body nor have negative concentrations. To account for this physical limitation, we constrain the input and output as follows:

$$\begin{aligned} u(t) &\geq 0, \quad \forall t > 0, \\ y(t) &\geq 0, \quad \forall t > 0. \end{aligned}$$

To obtain the control sequence, we solve the following optimization problem:

$$u(t+i|t)|_i^M = \arg \min_{u(t+i|t)} \Omega. \quad (11)$$

Although a feasible solution  $u(t+i|t)|_i^M$  is obtained for the horizon  $M$ , only the first term  $u(t|t)$  will be implemented, and at time  $t+1$ , the optimization procedure will be repeated. We solve the optimization problem (11) online using the MATLAB Model Predictive Control toolbox to obtain a control policy that satisfactorily tracks the desired reference signal.

We present controller performance for two informative cases. For the following two simulations, the system dynamics (Figure 3) model those of an actual trauma patient. We fit the parameters of the nonlinear model (3), which constitutes the system dynamics, to CAT experiment data for one of the 40 trauma patient samples in Dataset 2, who we will call Trauma Patient 1. Therefore, the model output represents the unique response of that patient. The MPC process model that we use is the ARX model that we previously identified, (8). The sampling time for the following simulations is set to  $1/3$  minutes = 20 seconds, which is equal to the CAT experiment measurement sampling period. For these two simulations, we assume that the input delay is zero, simply to check SISO MPC feasibility.

**Case 1:** This case represents a recovery of thrombin concentration in injured humans to a value that is within our stipulated normal region. The reference that we wish to track is

$$y_{r_1} = 130 (\tanh^2(0.1t)) \times 10^{-9} \text{ M}. \quad (12)$$

The steady-state value of this signal, 130 nM, is the mean thrombin peak value of normal samples (Figure 4). As thrombin is not initially present in a healthy human blood stream, we set the initial concentration of thrombin and the reference start point to zero for this simulation. Figure 5 shows that the controller periodically pulses TF inputs to achieve satisfactory thrombin tracking for this case. The output thrombin concentration remains within the upper and lower boundary lines that define the minimum and maximum normal concentration of thrombin, which we obtained from the thrombin peak concentrations of 20 normal samples in Dataset 1. In Figure 4, the peak value of the minimum is 68 nM, and the peak value of the maximum is 210 nM.

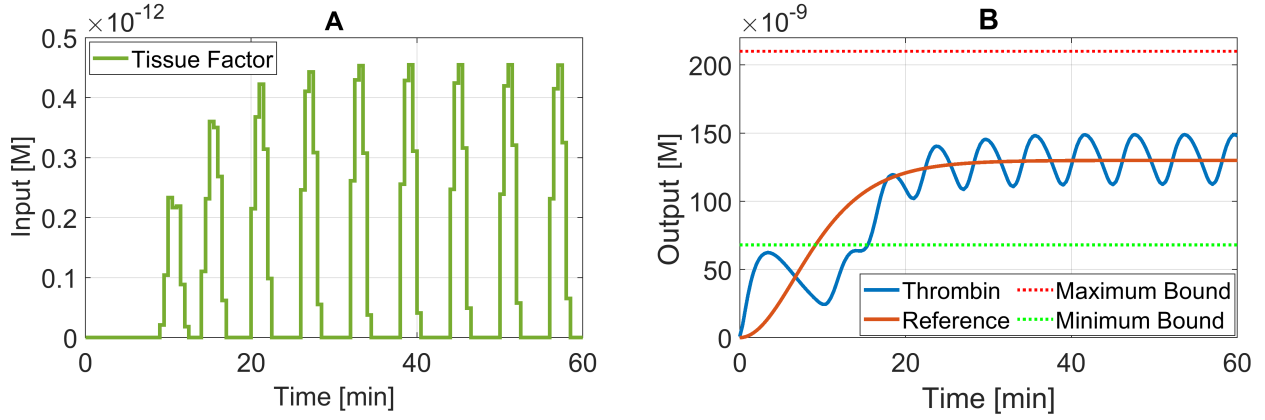


**FIGURE 5** MPC of coagulation using a single TF input to regulate a constant output concentration of thrombin. The system dynamics capture those of Trauma Patient 1. The system input delay is assumed to be zero. (A) The controller sequence of delivered TF. (B) Thrombin generation with satisfactory reference tracking. The output thrombin concentration is within the minimum and maximum bounds of normal.

**Case 2:** We choose a sinusoid reference signal to assess controller robustness to references that may vary depending on patient clinical condition:

$$y_{r_2} = (130 + 30 \sin(0.17t)) \times 10^{-9} \text{ M.} \quad (13)$$

An example where this case is useful is in infection-induced coagulopathy in the lung, such as that arising during COVID-19 infection, which can cause substantial blood clots in the lung<sup>39</sup>. Since thrombin acts as both anticoagulant and procoagulant, a varying concentration can reduce clot formation and also regulate bleeding. To differentiate this scenario from Case 1, we start the simulation from a non-zero initial thrombin concentration. Figure 6 shows the designed MPC controller signal of periodically pulsed TF inputs with a periodic time-varying magnitude, and the resultant satisfactory reference tracking. The output thrombin concentration is nearly always within the minimum and maximum normal concentration limits, but three small excursions occur.

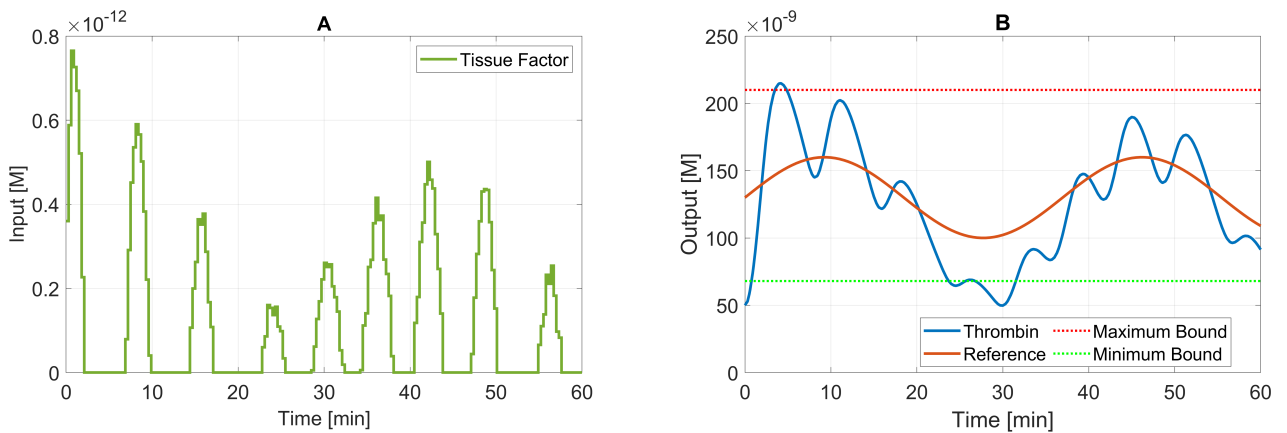


**FIGURE 6** MPC of coagulation using a single TF input to regulate a time-varying output concentration of thrombin. The system dynamics capture those of Trauma Patient 1. The system input delay is assumed to be zero. (A) The controller sequence of delivered TF. (B) Thrombin generation with satisfactory reference tracking. The output thrombin concentration is mostly within the minimum and maximum bounds of normal, although three small excursions occur.

## 4 | MULTI-INPUT SINGLE-OUTPUT MODEL PREDICTIVE CONTROL

A trauma patient's coagulation behavior can often fluctuate between hypo- and hyper-coagulable states during TIC recovery<sup>6</sup>. Since removing excessive thrombin to address hyper-coagulation (thrombosis) is not feasible, a potential solution is to instead add proteins that reduce and inhibit coagulation cascade activity. In a SISO system setup, high thrombin levels decay only passively from natural system dynamics. With the use of multiple coagulation factor concentration inputs, high thrombin levels can be reduced actively, and a controller can also leverage the unique effects of intermediate coagulation factors on coagulation dynamics to quickly achieve reference tracking from low thrombin levels. Accordingly, we investigate the feasibility of MPC to treat TIC such that output thrombin levels are regulated by multiple input coagulation factor concentrations. This MISO scheme steps toward the desired TIC treatment vision.

One of the benefits of the nonlinear model developed in Section 2 is its unique structure: states of the system represent individual coagulation factors rather than protein complexes. Hence, it is possible to use individual coagulation factors as distinct inputs, forming a MISO system. We modify the coagulation model (3) for multiple inputs:

$$\begin{aligned}\dot{x}_1(t) &= -K_{d_1}x_1(t) - \beta x_1(t)x_2(t) + u_1(t), \\ \dot{x}_2(t) &= K_{p_2} - K_{d_2}x_2(t) - \beta x_1(t)x_2(t) + u_2(t), \\ \dot{x}_3(t) &= \gamma x_1(t)x_2(t) - K_{d_3}x_3(t) + u_3(t), \\ \dot{x}_4(t) &= K_{n_4}x_3(t) - K_{d_4}x_4(t),\end{aligned}\tag{14}$$

where  $u_1(t)$ ,  $u_2(t)$ , and  $u_3(t) \in \mathbb{R}^+$  are three concentration system inputs: TF, factor VII, and factor Xa, respectively. Since we lack experimental thrombin measurements from a multi-input perspective, we cannot form an ARX model by system identification as we did in Section 3 to enable our MPC scheme to estimate plant output. Instead, we obtain a process model by using the Jacobian of our nonlinear model, i.e., a linear state space representation around the typical equilibrium point.

### 4.1 | Model Predictive Control Design and Performance

The cost function in (10) can be expanded for multiple inputs:

$$\Omega \triangleq \sum_{k=1}^N \alpha_1 (y_r(t+k) - \hat{y}(t+k|t))^2 + \sum_{q=1}^P \left[ \sum_{i=0}^M \left[ \alpha_{2_q} (u_q(t+i|t))^2 + \alpha_{3_q} (\Delta u_q(t+i|t))^2 \right] \right],\tag{15}$$

where  $P \in \mathbb{R}^+$  is a positive integer that indicates the number of inputs.

The selected weights of the objective cost function (15) are

$$\text{Output: } \alpha_1 = 2.5, \quad \text{Input: } \begin{cases} \alpha_{2_1} = 0.3, \\ \alpha_{2_2} = 0.4, \\ \alpha_{2_3} = 0.3, \end{cases} \quad \text{Input Change Rate: } \begin{cases} \alpha_{3_1} = 0.1, \\ \alpha_{3_2} = 0.1, \\ \alpha_{3_3} = 0.1. \end{cases}$$

We select the output to have the highest weight ( $\alpha_1$ ) to ensure that close tracking of the thrombin reference occurs. The second input, factor VII, has a slightly larger weight ( $\alpha_{2_2}$ ) compared to the other inputs to avoid an initial spike in its concentration, because this input has a non-zero steady state value in normal samples. The weights for changes to the input rates ( $\alpha_{3_i}$ ) are equal and selected to prevent shocks in the dynamic system response.

We define the following constraints to account for the same physical limitations as before:

$$\begin{aligned}u_p(t) &\geq 0, \text{ for } P = 1, 2, 3, \forall t > 0, \\ y(t) &\geq 0, \forall t > 0.\end{aligned}$$

To obtain the set of control sequences  $\mathbb{U}$  for  $M$  control horizons, we solve the following optimization problem for the cost function (15):

$$\{u_1(t+i|t)|_i^M, u_2(t+i|t)|_i^M, \dots, u_q(t+i|t)|_i^M\} = \arg \min_{u(t+i|t)} \Omega.\tag{16}$$

We solve this optimization problem using the MATLAB Model Predictive Control toolbox.

We choose reference signal (13), a time-varying sinusoidal signal, to evaluate MISO MPC performance. For the simulations in this section, we again assume that the input delay is zero, simply to check MISO MPC feasibility. We take the sampling period to be 1 minute, a realistic expectation of the period in a practical implementation. Figure 7 confirms that reference tracking is

satisfactory using the designed MPC scheme for Trauma Patient 1. Moreover, this simulation depicts the advantage of a multi-input approach to satisfactory reference tracking compared to the single-input case, despite the longer sampling period. Unlike Figure 6, there are no output oscillations from natural decay dynamics, nor are there any excursions outside normal bounds.

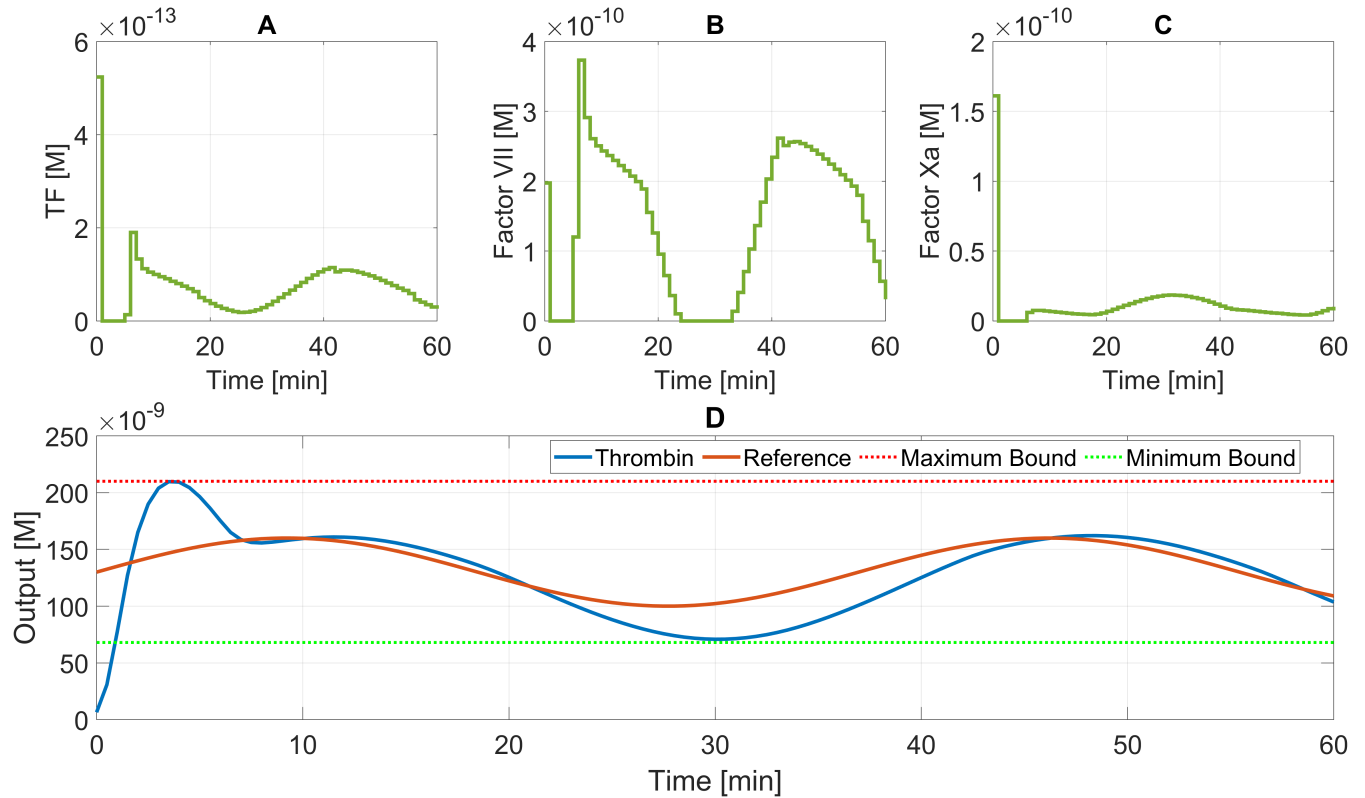


**FIGURE 7** MPC of coagulation using multiple coagulation factor inputs to regulate a time-varying output concentration of thrombin. The system dynamics capture those of Trauma Patient 1. The system input delay is assumed to be zero. (A) The controller sequence for the first input, delivered TF. (B) The controller sequence for the second input, delivered factor VII. (C) The controller sequence for the third input, delivered factor Xa. (D) Thrombin generation with satisfactory reference tracking, despite an increased sampling time. The output thrombin concentration stays within the minimum and maximum bounds of normal.

To further evaluate the efficacy of the presented MISO MPC scheme, we simulate thrombin regulation for four more trauma patients without changing controller parameters (weights, optimization function, and process model). For each simulation, the parameters of the system dynamics are a fit of the nonlinear coagulation model (3) to CAT experiment data for a unique trauma patient in Dataset 2. Figure 8A shows the parameter differences for all five trauma patients. Simulation results in Figure 8B confirm the capability of the proposed controller to regulate thrombin within normal bounds across different trauma patients.

A

Nonlinear Model Parameters							
Sample	$K_{d_1}$	$K_{d_2}$	$K_{d_3}$	$K_{d_4}$	$K_2$	$\beta \times 10^6$	$\gamma \times 10^9$
Trauma Patient 1	0.3206	0.0180	0.0153	0.3206	181.8834	293.6418	177.23
Trauma Patient 2	0.6148	0.0176	0.0204	1.2789	121.0734	103.78	119.43
Trauma Patient 3	0.4766	0.0178	0.0129	1.0247	368.3489	94.226	22.756
Trauma Patient 4	0.3715	0.0159	0.0118	0.7741	705.8072	65.120	4.0960
Trauma Patient 5	0.4189	0.0154	0.0171	0.5569	325.7994	18.958	94.686

B

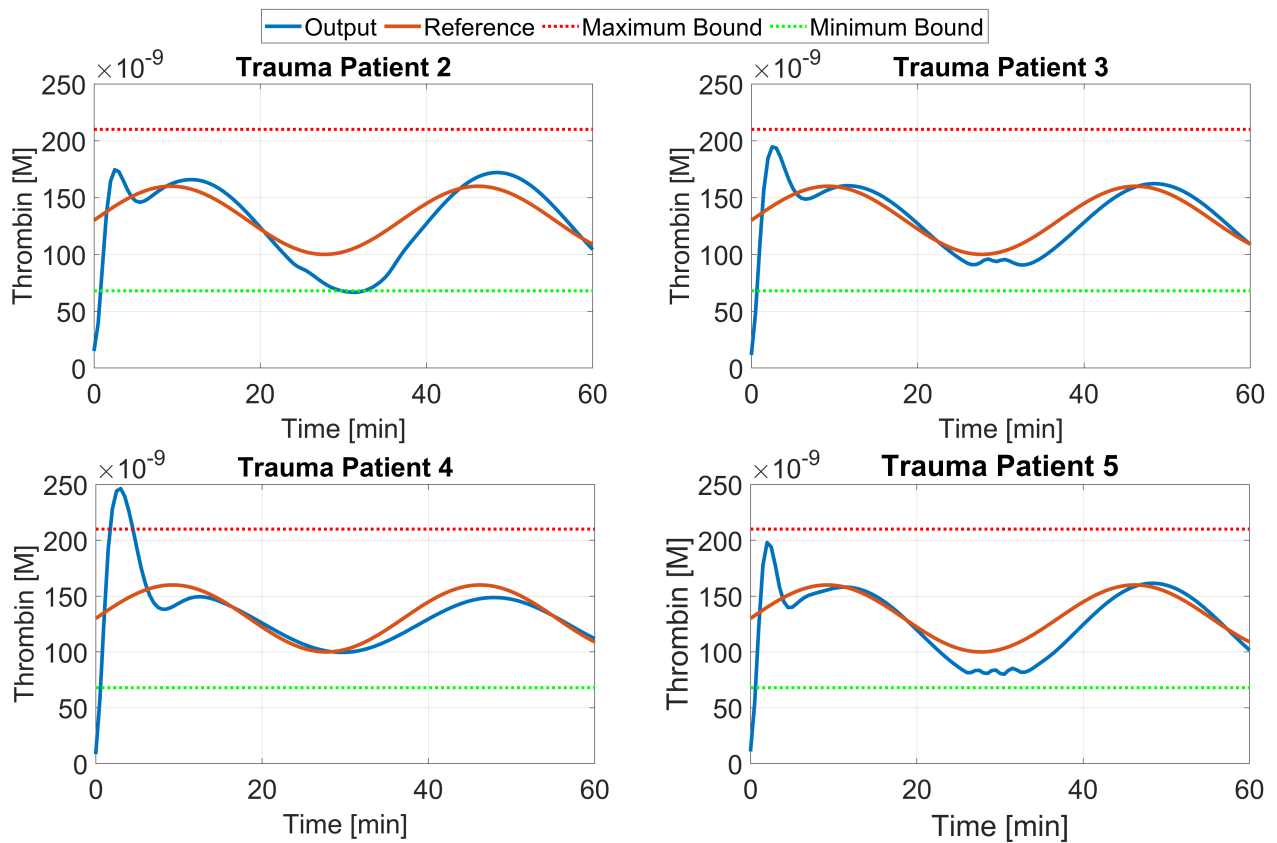


**FIGURE 8** MPC of coagulation using multiple coagulation factor inputs to regulate a time-varying output concentration of thrombin for different trauma patients. Each system's input delay is assumed to be zero. (A) Parameters of the nonlinear model (3) for five different trauma patients from fits to experimental CAT data. (B) Satisfactory thrombin reference tracking for four trauma patients different from Figure 7 using the same MISO MPC controller as in Figure 7. Satisfactory reference tracking within normal bounds across multiple simulated patients confirms controller efficacy.

## 5 | ROBUST MODEL PREDICTIVE CONTROL

The coagulation process is subject to characteristic nonlinearities that must be compensated for, including input saturation and an unknown state-dependent power law input delay  $\tau$  that is a function of TF (state  $x_1$  in (3))<sup>27</sup>, Figure 9:

$$\tau = \sigma x_1^{-\eta}, \quad (17)$$

where  $\sigma \in \mathbb{R}^+$  and  $\eta \in \mathbb{R}^+$  are positive constants. In this section, we evaluate the performance of our previously designed MPC schemes in the presence of input time delay (17). The magnitude of this time delay is particularly problematic when it is of the same order as the system's time-constant.

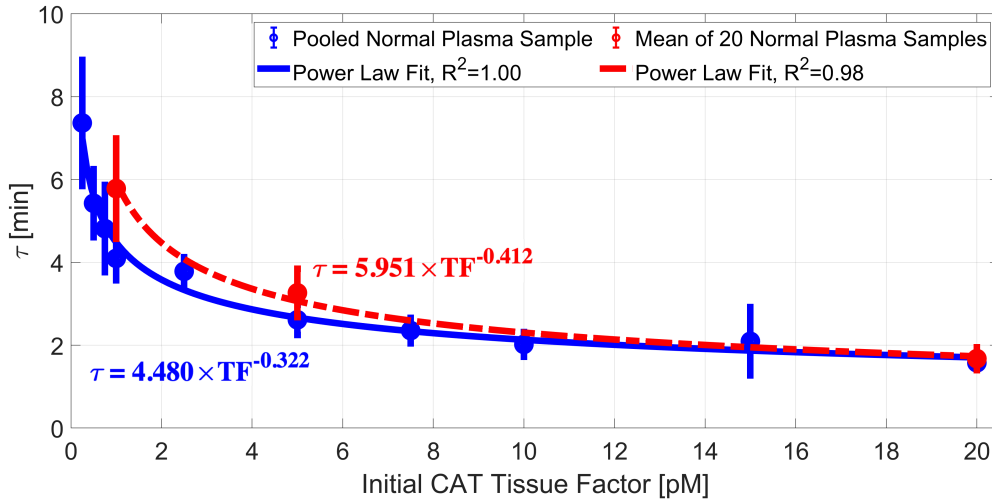


**FIGURE 9** Time delay in the human coagulation model (3). Time delays extracted from CAT experiment data are correlated with input TF concentration via a power law. Red indicates biological replicates from 20 different normal plasma samples ( $R^2 = 1.00$ ), Dataset 1, blue corresponds to technical replicates on a pool of normal plasma samples ( $R^2 = 0.98$ ).

Elsewhere, we designed a satisfactory positive system controller, Figure 10A–C, using a Lyapunov analysis<sup>27</sup>. We now compare the performance of our designed MPC schemes from Sections 3 and 4 to this state-of-the-art nonlinear controller for the system dynamics of Trauma Patient 1. We perform MPC simulations from the same initial conditions as Figure 10A–C where the initial thrombin level is elevated at 300 nM, a condition that is commonly observed in patients with hyper-coagulability. We again seek to track reference (13) and recover normal clotting.

The SISO MPC reference tracking results, Figure 10D–F, are no longer satisfactory due to the apparent phase shift that results from the input time delay. This input delay can exceed six minutes, which is much higher than the approximately one minute delay experienced by the nonlinear controller based on its choice of TF concentration system input. The poor performance and observed substantial violation of normal bounds may be attributed to the lack of any time-delay representation in the designed MPC, since the identified ARX model only considers a small constant time delay. Our prior work Figure 10C shows a much closer tracking of the reference because the input delay structure (17) is included in the nonlinear controller design. We anticipate improving our SISO MPC results in future work by considering input nonlinearities, such as a state-dependent time delay, in the model predictive controller design.

In the MISO MPC case with a time delay (17) imposed on the first state TF, the reference tracking results, Figure 10E–G, show closer thrombin trajectory following than our Lyapunov controller. This tracking occurs in spite of a high input delay of about five minutes. The observed excellent performance within normal bounds attests to the ability of cocktails of coagulation factors to compensate for nonlinearities in the clotting process. These results confirm that there is a robustness benefit to using intermediate coagulation factors when automating TIC treatment, to overcome unmodeled disturbances.

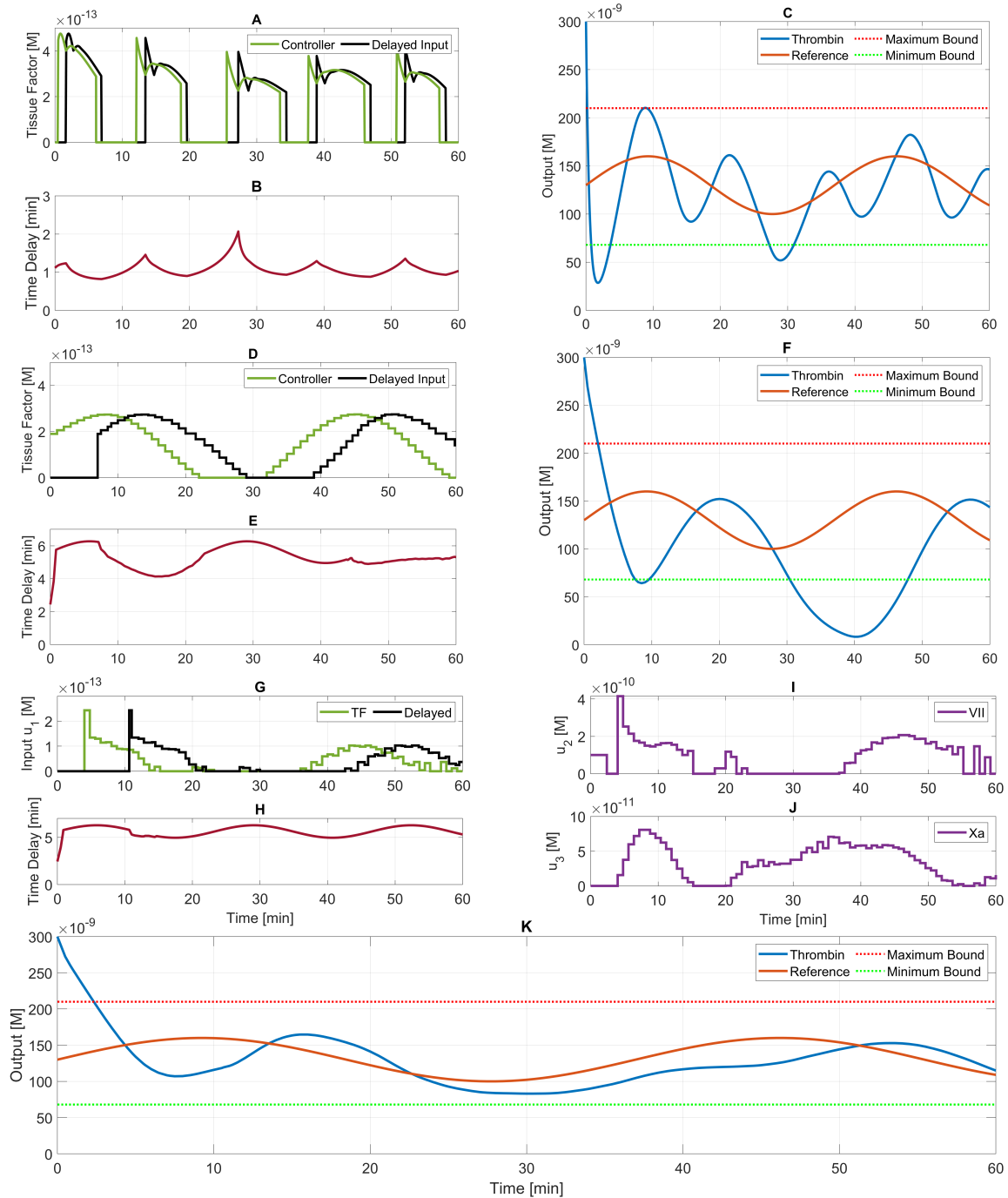


**FIGURE 10** SISO and MISO MPC performance comparison with a state-of-the-art positive system controller in the presence of an unknown state-dependant power law input delay<sup>27</sup> for the system dynamics of Trauma Patient 1. (A) TF signal from the controller in the literature<sup>27</sup>. (B) The input time delay associated with the signal in panel A is between one and two minutes. (C) Tracking performance due to the controller TF signal in panel A. (D) The SISO MPC controller sequence of delivered TF. The green line indicates the controller signal and the black line shows the delayed input. (E) The input time delay associated with the signal in panel D. This time delay is substantial, at around five minutes. (F) Tracking performance due to the controller TF signal in panel D shows a phase lag (horizontal shift) and constraint violation. (G) MISO MPC input TF sequence  $u_1$  (green line) and the corresponding power-law state-dependent delayed input (black line). (H) The input time delay associated with the signal in panel G is again substantial at around five minutes. (I) MISO MPC input sequence  $u_2$ , factor VII. (J) MISO MPC input sequence  $u_3$ , factor Xa. (K) Tracking performance due to the controller signals in panels G, I and J is better than the state-of-the-art in panel C, and does not violate normal bounds. Inputs  $u_2$  and  $u_3$  compensate for the delayed input signal  $u_1$ . The bounds define the minimum (68 nM) and maximum (210 nM) normal concentration of thrombin, obtained from normal samples.

## 6 | CONCLUSIONS AND FUTURE WORK

In this article, we first developed a novel nonlinear control-oriented model of coagulation for use in closed-loop TIC treatment. This model overcomes the limitations of existing models, namely, high computational expense and uncontrollable (in practice) states. The states in our new model have biochemical kinetic meaning, and facilitate multiple independent coagulation factor concentration manipulation. Our nonlinear model also preserves an ability to accurately capture thrombin generation, and hence clotting behavior, in trauma patients when compared to a simple linear phenomenological model in the literature, because our new model is a generalization of that literature model.

We then showed that SISO MPC, which uses a TF concentration input to regulate thrombin, and MISO MPC, which adds concentrations of factors VII and Xa as input, accomplish satisfactory thrombin reference tracking. Our controllers leverage our new nonlinear coagulation model. Our MISO MPC is also robust to an experimentally observed nonlinearity, a state-dependent power law input delay, because the additional coagulation factor concentration inputs in the controller provide increased compensation capability.

We anticipate improving the results in this article by incorporating learning-based and adaptive MPC techniques, to account for the high uncertainty in trauma patient coagulation dynamics, and to update the nonlinear plant online as new coagulation factor concentration measurements become available. We also intend to study TIC treatment over longer horizons, e.g., the first 24 hours post-hospitalization, or during a patient's entire ICU stay, both of which will increase clinical relevance and further personalize interventions at the point-of-care. Finally, we will explore applications to other coagulopathy conditions beyond TIC.

## CONFLICT OF INTEREST

The authors declare that they have no conflict of interest.

## DATA AVAILABILITY

The data that support the findings of this study are openly available<sup>25</sup> at: <https://doi.org/10.1126/scitranslmed.aaf5045>

## ORCID

Damon E. Ghetmiri <https://orcid.org/0000-0003-4726-4663>

Amor A. Menezes <https://orcid.org/0000-0003-3923-5766>

## References

1. Buchman TG, Billiar TR, Elster E, et al. Precision medicine for critical illness and injury. *Critical Care Medicine* 2016; 44(9): 1635–1638.
2. Gonzalez E, Moore HB, Moore EE. *Trauma Induced Coagulopathy*. Springer . 2016.
3. Centers for Disease Control and Prevention . 10 Leading Causes of Death, United States. <https://wisqars-viz.cdc.gov/8006/lcd/home>; 2019.
4. Rhee P, Joseph B, Pandit V, et al. Increasing trauma deaths in the United States. *Annals of Surgery* 2014; 260(1): 13–21.
5. Stiell IG, Nesbitt LP, Pickett W, et al. The OPALS Major Trauma Study: impact of advanced life-support on survival and morbidity. *Canadian Medical Association Journal* 2008; 178(9): 1141–1152.
6. Moore EE, Moore HB, Kornblith LZ, et al. Trauma-induced coagulopathy. *Nature Reviews Disease Primers* 2021; 7(1): 1–23.
7. Peng N, Su L. Progresses in understanding trauma-induced coagulopathy and the underlying mechanism. *Chinese Journal of Traumatology* 2017; 20(3): 133–136.

8. Maegele M, Paffrath T, Bouillon B. Acute traumatic coagulopathy in severe injury: incidence, risk stratification, and treatment options. *Deutsches Ärzteblatt International* 2011; 108(49): 827.
9. Cohen MJ. Coagulation Perturbations After Severe Injury: Translational Approaches and the State of the Science. In: Springer. 2018 (pp. 215–221).
10. Bradley M, Shi A, Khatri V, et al. Prediction of venous thromboembolism using clinical and serum biomarker data from a military cohort of trauma patients. *BMJ Mil Health* 2020.
11. Holcomb JB, Tilley BC, Baraniuk S, et al. Transfusion of plasma, platelets, and red blood cells in a 1: 1: 1 vs a 1: 1: 2 ratio and mortality in patients with severe trauma: the PROPPR randomized clinical trial. *The Journal of the American Medical Association* 2015; 313(5): 471–482.
12. Cantle PM, Cotton BA. Prediction of Massive Transfusion in Trauma. *Critical Care Clinics* 2017; 33(1): 71–84.
13. Sommer N, Schnüriger B, Candinas D, Haltmeier T. Massive transfusion protocols in nontrauma patients: A systematic review and meta-analysis. *Journal of Trauma and Acute Care Surgery* 2019; 86(3): 493–504.
14. Adams RL, Bird RJ. Coagulation cascade and therapeutics update: relevance to nephrology. Part 1: Overview of coagulation, thrombophilias and history of anticoagulants. *Nephrology* 2009; 14(5): 462–470.
15. Narayanan S. Multifunctional roles of thrombin. *Annals of Clinical & Laboratory Science* 1999; 29(4): 275–280.
16. Giangrande P, Andreeva T, Chowdary P, et al. Clinical evaluation of glycoPEGylated recombinant FVIII: efficacy and safety in severe haemophilia A. *Thrombosis and Haemostasis* 2017; 117(02): 252–261.
17. Giangrande P, Peyvandi F, O'Mahony B, et al. Kreuth IV: European consensus proposals for treatment of haemophilia with coagulation factor concentrates. *Haemophilia* 2017; 23(3): 370–375.
18. Klages M, Zacharowski K, Weber CF. Coagulation management in trauma-associated coagulopathy: allogenic blood products versus coagulation factor concentrates in trauma care. *Current Opinion in Anesthesiology* 2016; 29(2): 245–249.
19. Innerhofer P, Fries D, Mittermayr M, et al. Reversal of trauma-induced coagulopathy using first-line coagulation factor concentrates or fresh frozen plasma (RETIC): a single-centre, parallel-group, open-label, randomised trial. *The Lancet Haematology* 2017; 4(6): e258–e271.
20. Gratz J, Ponschab M, Iapichino GE, et al. Comparison of fresh frozen plasma vs. coagulation factor concentrates for reconstitution of blood: An *in vitro* study. *European Journal of Anaesthesiology| EJA* 2020; 37(10): 879–888.
21. Dutton RP, McCunn M, Hyder M, et al. Factor VIIa for correction of traumatic coagulopathy. *Journal of Trauma and Acute Care Surgery* 2004; 57(4): 709–719.
22. Joseph B, Amini A, Friese RS, et al. Factor IX complex for the correction of traumatic coagulopathy. *Journal of Trauma and Acute Care Surgery* 2012; 72(4): 828–834.
23. Turpie AG. Oral, direct factor Xa inhibitors in development for the prevention and treatment of thromboembolic diseases. *Arteriosclerosis, Thrombosis, and Vascular Biology* 2007; 27(6): 1238–1247.
24. Ghetmiri DE, Cohen MJ, Menezes AA. Personalized modulation of coagulation factors using a thrombin dynamics model to treat trauma-induced coagulopathy. *npj Systems Biology and Applications* 2021; 7: 44.
25. Menezes AA, Vilardi RF, Arkin AP, Cohen MJ. Targeted clinical control of trauma patient coagulation through a thrombin dynamics model. *Science Translational Medicine* 2017; 9(371): eaaf5045.
26. Luan D, Szlam F, Tanaka KA, Barie PS, Varner JD. Ensembles of uncertain mathematical models can identify network response to therapeutic interventions. *Molecular BioSystems* 2010; 6(11): 2272–2286.
27. Ghetmiri DE, Menezes AA. Control of positive systems with an unknown state-dependent power law input delay and input saturation. 2022.

28. Rawlings JB, Mayne DQ, Diehl M. *Model Predictive Control: Theory, Computation, and Design*. Nob Hill Publishing. Second ed. 2017.
29. Parker RS, Doyle FJ, Peppas NA. A model-based algorithm for blood glucose control in type I diabetic patients. *IEEE Transactions on Biomedical Engineering* 1999; 46(2): 148–157.
30. Ellingsen C, Dassau E, Zisser H, et al. Safety constraints in an artificial pancreatic  $\beta$  cell: an implementation of model predictive control with insulin on board. *Journal of Diabetes Science and Technology* 2009; 3(3): 536–544.
31. Allgöwer F, Zheng A., eds. *Nonlinear model predictive control*. 26 of *Progress in Systems and Control Theory*. Birkhäuser . 2000.
32. Köhler J, Kötting P, Soloperto R, Allgöwer F, Müller MA. A robust adaptive model predictive control framework for nonlinear uncertain systems. *International Journal of Robust and Nonlinear Control* 2020.
33. Hockin MF, Jones KC, Everse SJ, Mann KG. A model for the stoichiometric regulation of blood coagulation. *Journal of Biological Chemistry* 2002; 277(21): 18322–18333.
34. Hemker H, Giesen P, AIDieri R, et al. The calibrated automated thrombogram (CAT): a universal routine test for hyper- and hypocoagulability. *Pathophysiology of Haemostasis and Thrombosis* 2002; 32(5-6): 249–253.
35. Lyzell C. *Initialization methods for system identification*. PhD thesis. Linköping University, Linköping, Sweden; 2009.
36. Ljung L. *System Identification Toolbox: User's guide*. The MathWorks, Inc . 2014.
37. James G, Witten D, Hastie T, Tibshirani R. *An Introduction to Statistical Learning: with Applications in R*. Springer . 2013.
38. Pintelon R, Schoukens J. *System Identification: A Frequency Domain Approach*. John Wiley & Sons . 2012.
39. D'Agnillo F, Walters KA, Xiao Y, et al. Lung epithelial and endothelial damage, loss of tissue repair, inhibition of fibrinolysis, and cellular senescence in fatal COVID-19. *Science Translational Medicine* 2021; 13(620): eabj7790.

